PCCP

Accepted Manuscript

ROYAL SOCIETY OF CHEMISTRY

www.rsc.org/pccp

Physical Chemistry Chemical Physics
CREATED USING THE RSC LaTeX PCCP ARTICLE TEMPLATE – SEE www.rsc.org/electronicfiles FOR DETAILS
ARTICLE TYPE www. rsc.org/xxxxxx | XXXXXXXX

Role of hydration in phosphatidylcholine reverse micelle structure and gelation in cyclohexane: a molecular dynamics study

S. Vierros,[a] and M. Sammalkorpi*[a]

Received Xth XXXXXXXXXX 20XX, Accepted Xth XXXXXXXXX 20XX
First published on the web Xth XXXXXXXXXX 200X
DOI: 10.1039/b000000x

In this work, we employ all-atom molecular dynamics simulations to examine the hydration response of phospholipid reverse micelles in cyclohexane. This ternary phospholipid / water / cyclohexane system is an important organogel forming system and the focus of this study is on gaining insight on the factors governing the gelation transition. We map the contributions rising from specific lipid - lipid and lipid - water interactions, and their response to increasing aggregate size and changes in water-to-lipid ratio. We find that, opposed to phospholipid / heptane organogels, in cyclohexane, lipid bridging and hydrogen bond driven stabilization of the lipid head group packing is at minor role in dictating the reverse micelle structural transitions corresponding to the organosol / organogel phase transition in this system. Instead, increasing the lipid head hydration changes the lipid packing factor directly which leads to gelation through the formation of long, wormlike micelles. Furthermore, the confined environment in the reverse micellar cores slows down the water dynamics significantly in comparison to fully hydrated phospholipid bilayers and at low water-to-lipid ratios this slow-down is even more significant. The findings map the role of hydration at microscopic level in these systems and could enable tailoring reverse micellar systems for applications relying on the structure and dynamics of the reverse micelles. Examples include such as drug transport, nanotemplating, or confined chemistry in the reverse micelle core water space, e.g., in catalysis.

1 Introduction

Reverse micelles formed by amphiphilic self-assembly in apolar media provide highly dynamic and responsive aggregates with applications ranging from drug delivery systems and soft-templation of nanomaterials[1–3] to enhanced protein separation and structural stabilization[4]. In particular, lecithin reverse micelles have attracted much attention due to their biocompatibility and the unusual property of undergoing a phase transition from a freely running organosol state into a stiff, highly viscous organogel state[5]. This transition is generally attributed to the formation and entanglement of wormlike reverse micelles[6–8], and is typically controlled by a gelation agent. The list of compounds demonstrated to induce gelation in lecithin systems includes bile acids and salts[9,10], alkaline earth and rare earth cations[11,12], as well as, small polar molecules[13] including water[5] (see Ref. 14 for a comprehensive list).

Of these, the ternary systems of lecithin/water/oil are particularly interesting as the water-filled interior effectively permits solubilization of aqueous species in organic solvent, as well as, provides a confined space to perform aqueous chemistry, e.g. inorganic nanoparticle synthesis. In these systems, lecithin is a mixture of phosphatidylcholine (PC) lipids differing by their hydrocarbon tail length and degree of saturation, oil refers to an organic apolar solvent such as alkanes and fatty acid esters, and water acts as the gelation agent. The microstructure and macroscopic phase behaviour of lecithin/water/oil systems has been shown to be dependent on and controllable by factors such as temperature, lecithin composition (lipid tail structure) and water-to-lipid ratio, $w_0 = [water]/[lipid]$ where the square brackets refer to concentration[4,5,15]. The size of the reverse micelles, and through it the viscosity of lecithin/oil/water systems, is dominantly controlled by the water-to-lipid ratio in the system. On the other hand, an increase in the temperature decreases the mean micelle size through entropy gain. This decrease in micelle size lowers the viscosity. However, the effect of temperature can be partially nullified by introducing more saturated lipids into the system. Jointly, these signify the actual size distribution of the cylindrical wormlike reverse micelles is determined by the balance in free energy between the total entropic gain in splitting the aggregates into smaller sizes and the energetic penalty associated with the formation of end-caps to the finite size aggregates.

Characterisation of lecithin/water/oil organogels using scattering techniques[6–8,16,17], nuclear magnetic resonance spectroscopy[15,18,19] and rheology[20] has revealed that the internal structure of the organogel phase is determined by the chemical nature of the solvent. For example in cyclohexane water triggers uni-axial growth of the initially spherical reverse micelles

[a] *Department of Chemistry, Aalto University, P.O. Box 16100, 00076 Aalto, Finland. E-mail: maria.sammalkorpi@aalto.fi; Tel: +358-50-371 7434*

into disconnected wormlike reverse micelles. Maximum viscosity is attained around water-to-lipid ratio $w_0 = 11$ followed by a second shape transition to water-in-oil microemulsion droplets at $w_0 = 14$. The maximum water uptake in cyclohexane is around $w_0 = 24$ followed by phase separation into microemulsion phase and excess water phase [19]. On the other hand, in iso-octane, the growth of the reverse micelles with increasing hydration is much faster and maximum viscosity is attained already around $w_0 = 2$. Further addition of water increases first branching and around $w_0 = 4$ a phase separation into a stiff gel and a dilute organic phase occurs [21]. Solvents similar to iso-octane, such as n-decane and n-heptane, show analogous behaviour although details vary [13,19].

The striking difference in phase behaviour between lecithin organogels having organic solvents with similar size and composition (iso-octane vs. cyclohexane) as the continuous phase has risen the question of what exactly happens at the aggregate cores that induces the gelation. Clearly, water-to-lipid ratio is at key role in both cyclohexane and in solvents like iso-octane or heptane. It is generally thought that hydrogen bonding in apolar media can greatly promote lipid aggregation and this could result in the observed gelation. Indeed, several studies utilising infrared (IR) spectroscopy [13,22–24] have shown that the degree of hydrogen bonding in lecithin headgroups increases as a function of water-to-lipid ratio. However, the relation of these findings to the occurring gelation is not well understood. So far, Shchipunov and Shumilina [13] have provided the clearest picture on the mechanism of gelation in lecithin/water/heptane system using a series of water-like polar molecules. They were able to show that only sufficiently polar substances which are capable of forming multiple hydrogen bonds were effective at gelating lecithin/heptane solutions [13]. Shchipunov and Shumilina suggested that polar gelation agents, such as water, form a bridging structure that interlinks lipid headgroups. This stabilises the cylindrical structure of the wormlike reverse micelles, and enables their growth.

In line, Zhao et al. [22] have suggested that also in cyclohexane, hydrogen bond bridging is at decisive role in determining the lecithin aggregate morphology. However, their IR spectroscopic measurements on cyclohexane/lecithin/water system showed directly only that the degree of hydrogen bonding in the lecithin phosphate group is linked with the shape of the reverse micelles [22]. This leaves the lecithin gelation mechanism in cyclohexane an open question especially since the water-to-lipid ratios corresponding to gelation, and also subsequent phase behaviour between heptane and cyclohexane differ significantly.

The gelation mechanism at the level of specific interactions such as bridging is challenging to probe experimentally because of, e.g., spectral interference in IR measurements, as well as, difficulty in interpreting the results at the necessary microscopic detail. Computer simulations, and especially, molecular dynamics which readily enable studying both the microstructure and dynamics, have emerged as an increasingly popular tool to complement the experimental studies. Atomistic studies that enable the mapping of specific interactions in reverse micelle systems are, however, scarce. Aqueous reverse micelles have been examined by molecular simulations mainly for the ionic Aerosol OT surfactant [25,26] and non-ionic polyethylene glycol based surfactants [27]. These studies have probed the reverse micelle structure, as well as, the structure and dynamics of the contained water environment. Additionally, our earlier work on phosphatidylcholine reverse micelles in cyclohexane [28] assessed the force field accuracy on describing lecithin/cyclohexane systems. To our knowledge, lecithin reverse micelle hydration has not been examined by computational means prior to this work.

Here, we characterise the structure and hydration of lecithin (phosphatidylcholine) reverse micelles using atomistic-detail molecular dynamics with the aim of clarifying the role of hydration and bridging in the formation of lecithin/water/cyclohexane organogels. We examine a series of water-to-lipid ratios with reverse micelles of different size and analyse the influence of hydration in these systems. Furthermore, we quantify the formation, dynamics and significance of lipid-water hydrogen bonds, hydrogen bond bridges, as well as, their dynamics. Finally, we discuss the results in terms of the gelation mechanism of lecithin in cyclohexane and consider the implications of the findings on lecithin/water/oil gelating systems in general, as well as, on water as a gelating agent in these systems.

2 Methods

GROMACS 4.6 simulation package [29,30] was used for the simulations. Molecular interactions were modelled by the additive CHARMM force field [31]. Lipids were described using the CHARMM36 lipid parametrisation [32] while cyclohexane model was taken from the compatible carbohydrate force field from Ref. 33. Water is modelled using the CHARMM modified explicit TIP3P water model [31]. We originally chose the CHARMM36 force field, because the lipid model has been validated also at low hydration with the water model, verified parameters are available for both saturated and unsaturated lipids [32], and force field consistent parameters for cyclohexane exist [33,34]. However, our earlier work [28] indicates the cyclohexane penetration into the lipid tail region is underestimated in this description. We demonstrated this can be compensated by introducing extra *cis* bonds into the lipid tail to increase steric repulsion between the tails (as solvent penetration would). With 1,2-distearidonoyl-sn-glycero-3-phosphocholine (DSPC) as the lipid (4 unsaturated bonds in each tail, see Fig. 1), the model reproduces experimental characteristics of lecithin reverse micelles in cyclohexane at vary-

ing water-to-lipid ratios by core dimensions, water channel structure, and overall form[28]. However, the tail region structure, and especially the solvent interactions there, are likely to be to be unrealistic in the model. Consequently, the reverse micelle cross-section is smaller because the excess *cis* bonds shorten the acyl chains[28].

Periodic boundary conditions were applied in all three dimensions and long-range electrostatic interactions were calculated using the PME method[35], with a fourth-order smoothing spline. A real space cut-off of 1.2 nm and reciprocal space grid of 0.12 nm were used. Lennard-Jones potentials were smoothly shifted to zero between 0.8 nm and 1.2 nm. Equations of motion were integrated with the leap-frog algorithm using a time step of 2 fs and bonds involving hydrogen were constrained to their equilibrium distance using LINCS[36] and SETTLE[37] algorithms. A stochastic velocity rescaling thermostat[38] was used with reference temperature of 325 K and a relaxation time constant of 0.5 ps. Pressure was kept constant using Parinello-Rahman barostat[39] with a time constant of 4.0 ps. Pressure control was applied isotropically with compressibility set to $8.2{\cdot}10^{-5}$ bar^{-1}. System coordinates and energies were recorded every 10 ps. VMD[40] was used to generate all the simulation snapshots.

To study the hydration behaviour of lecithin as a function of water-to-lipid ratio w_0, water-to-lipid ratios of 5, 7 and 11 were examined for reverse micelles with aggregation numbers between 57 and 129. Aggregation number of a micelle specifies how many lipids form that particular micelle. Table 1 provides a summary of the simulated systems and Fig. 1 a snapshot showing a sample reverse micelle simulation configuration. The water-to-lipid ratio values were selected to sample the water-to-lipid range below the experimentally defined maximum macroscopic viscosity where the structure of the reverse micelles is known to be wormlike[7,8,19]. The aggregation numbers were chosen so that the larger aggregation numbers at water-to-lipid ratios 7 and 11 corresponded to a clearly elongated micelle (as opposed to spherical) yet small enough to allow simulations in all-atom detail. The smaller, clearly more spherical micelles enable evaluating the micelle size and form sensitivity of the findings. For comparison, also a fully hydrated ($w_0 = 28$) lipid bilayer structure composed of 128 lipids was characterised. Although the tail structure differs from naturally sourced lecithin, the equilibrated area per lipid in our simulations, 76.9 Å^2, is within the range expected based on experiments of lamellar lecithin assemblies[16]. The simulations were run $60-100$ ns.

Ideally, this type of simulations would start from a random mixture of the constituent molecules as the initial configuration. However, this type of approach requires the self-assembly process to equilibrate within simulationally accessible timescales. In the lecithin/oil systems, for example a 100 ns simulation starting from a random initial configuration allows only the initial micellisation to take place. As a simulation of these system sizes and timescales is typically run parallelized, in a cluster computer over an extended period of time, the formation and equilibration of any larger aggregates would take prohibitively long. Hence, to speed up equilibration, the reverse micelles were preassembled to an initially spherical form that is unbiased toward the cylindrical form the micelles adopt in the simulations. The procedure to prepare the initial configurations is detailed in Ref. 28.

The first 25 ns of the $w_0 = 11$ and $w_0 = 7$ simulations and was considered as the initial relaxation period and disregarded in the analysis. The $w_0 = 5$ simulation equilibrated slower because of the smaller amount of plasticizing water molecules and for it, the relaxation was 50 ns. Relaxation was measured as stabilization of the structural dimensions of the reverse micelles.

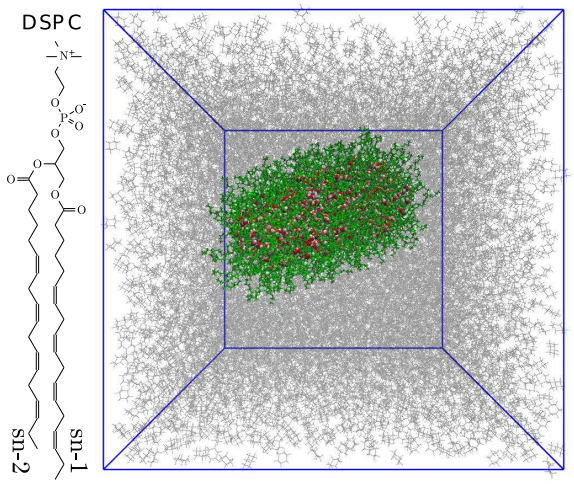

Fig. 1 At left, the structure of the 1,2-distearidonoyl-sn-glycero-3-phosphatidylcholine (DSPC) lipid. At right, a simulation snapshot corresponding to the final configuration of the system RM129.

Table 1 Summary of simulated reverse micellar and bilayer systems. The table presents the abbreviation used for the system, water-to-lipid ratio w_0, aggregation number N_{agg}, number of water molecules N_w, number of solvent molecules N_{CHX}, simulation duration t, and the size of the simulation box V

System	w_0	N_{agg}	N_w	N_{CHX}	t (ns)	V (nm^3)
RM70	5	70	350	6572	100	$11.0\times11.0\times11.0$
RM57	7	57	399	6765	87	$11.2\times11.2\times11.2$
RM78	7	78	546	6561	100	$11.3\times11.3\times11.3$
RM94	11	94	1034	8118	100	$12.1\times12.1\times12.1$
RM129	11	129	1419	9297	60	$12.7\times12.7\times12.7$
BL128	28	128	3584	0	65	$5.80\times5.80\times8.15$

In the analysis, we consider a hydrogen bond exists if the acceptor-hydrogen distance is less than 0.25 nm and the hydrogen-acceptor-donor angle is less than 30° . The distance cutoff is based on the first minimum in acceptor-hydrogen radial distribution function and the angle cutoff is equal to the default value for hydrogen bonds in GROMACS. To characterise the dynamics of the hydrogen bonds, we calculated so-called history-independent correlation functions. History-independent correlation functions express the conditional probability of a randomly selected pair of atoms being hydrogen bonded at time t provided that they were bonded at time $t = t_0$. Formally the correlation function $C_h(t)$ is given by[41]

$$C_h(t) = \frac{\langle h_{ij}(t_0)h_{ij}(t)\rangle}{\langle h_{ij}(t_0)\rangle} \quad (1)$$

where the angle brackets denote an average over all atom pairs ij and time origins t_0. $h_{ij}(t)$ is the binary existence function that tells whether or not a pair of atoms is hydrogen bonded to one another at time t; if a hydrogen bond between atoms i and j is intact at time t, $h_{ij}(t) = 1$ and otherwise it is zero. The integral of the correlation function yields the correlation time τ_h, which can be interpreted as the hydrogen bond lifetime assuming that the decay is exponential[41]

$$\tau_h = \int_0^\infty C_h(t)dt \quad (2)$$

In practice, the decay is rarely exponential[41]. Nonetheless, the integral is useful in qualitative analysis of the hydrogen bond dynamics and used in this work to compare the relative stability of the hydrogen bonding.

The dynamics of the hydrogen bond bridges, which form when a water molecule is bound to two different acceptor sites, are characterised similarly to the regular lipid-water hydrogen bonds. Here, a binary function $b_{ijk}(t)$ expresses whether a hydrogen bond bridge involving acceptor oxygens i and j, and a water molecule k exists. A correlation function along the spirit of Eq. 1 is now given by

$$C_b(t) = \frac{\langle b_{ijk}(t_0)b_{ijk}(t)\rangle}{\langle b_{ijk}(t_0)\rangle} \quad (3)$$

3 Results

In our previous study, in which we assessed the force-field accuracy on describing lecithin/cyclohexane systems, we characterised the structural response of DSPC reverse micelles to hydration and validated it against available experimental data[28]. The initial structures of the simulated reverse micelles are spherical but during the course of the initial relaxation,

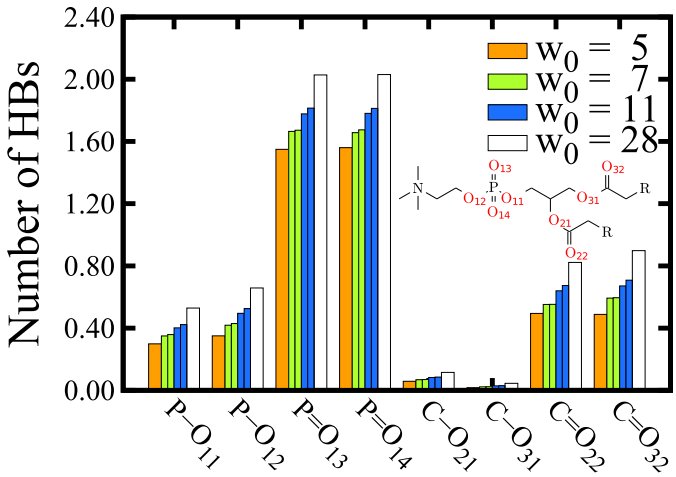

Fig. 2 Average number of hydrogen bonds (HBs) per different acceptor sites at different water-to-lipid ratios w_0. Where multiple aggregate sizes have been characterised at same w_0, data corresponding to the smaller aggregate is at left (see Table 1 for studied systems). The inset shows the structure of the phosphatidylcholine lipid head group to clarify the labelling of the acceptor sites. Error estimates according to block averaging are less than 0.01 except for $w_0 = 5$ where the error estimates are less than 0.02.

RM70 ($w_0 = 5$), RM78 ($w_0 = 7$), and RM129 ($w_0 = 11$) settle into a rod-like form with little fluctuations. However, the smaller reverse micelles RM57 ($w_0 = 7$) and RM94 ($w_0 = 11$) end fluctuating between spherical and rod-like forms in our simulations. Furthermore, the reverse micelles with equal water-to-lipid ratios have similar cross-sectional radii and the increase in aggregation number elongates the reverse micelle but does not change the core diameter. This signifies the reverse micelles undergo an axial elongation as their size increases which is in line with giant wormlike micelle form for the significantly larger aggregates present in experimental systems. On the other hand, an increase in w_0 increases the cross-sectional radii of the reverse micelles – again, in line with experimental observations[17].

Here, we characterise the role of water in this structural response. In particular, we map the specific interactions with the lipid head groups in the phosphatidylcholine reverse micelles. Figure 2 presents the average number of hydrogen bonds per acceptor site in the head groups. The number of hydrogen bonds at each acceptor site increases with increasing water-to-lipid ratio. This reflects increased access of the hydrogen bonding sites to water. The number of hydrogen bonds also shows a small dependence on the aggregation number of the reverse micelle. In line with this observation, Zhao et al. have reported that lipids in cylindrical reverse micelles form more hydrogen bonds than lipids in smaller spherical reverse mi-

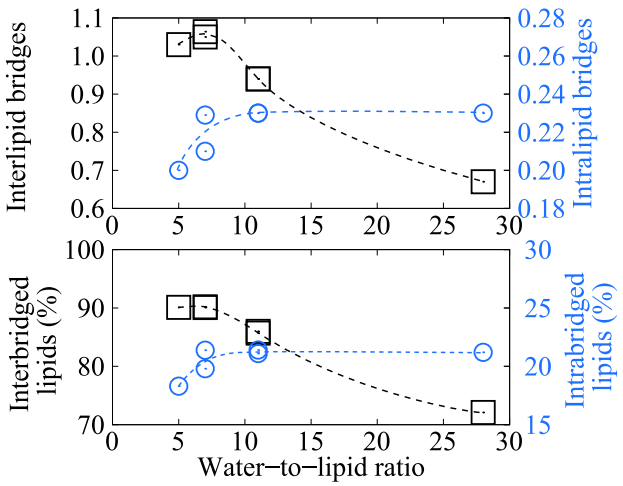

Fig. 3 The average number of interlipid (black squares) and intralipid (blue circles) bridges (top panel) and the average percentage of bridged lipids (bottom panel). An intralipid bridge signifies a water molecule is hydrogen bonded to two acceptor sites in the same lipid molecule whereas an interlipid bridge forms when a water molecule spans by hydrogen bonds two lipid molecules. Dashed lines are provided as visual guideline only. Error estimates according to block averaging are less than 0.01 (top panel) or 0.6 %-units (bottom panel).

celles[22].

In general, the data presented in Figure 2 shows the double bonded oxygen atoms (C=O and P=O) bind more water than the single-bonded oxygens (C–O and P–O) and oxygens in the phosphate group bind more water than similar oxygens in the glycerol moiety – irrespective of the water-to-lipid ratio. This signifies the hydrogen bonding is localised to phosphate group with tail carbonyl groups experiencing some hydration as well.

To quantify the hydrogen bond bridging, the average number and percentage of interlipid and intralipid bridges in the reverse micelles were calculated and compared to a fully hydrated bilayer, see Figure 3. A water molecule is considered to bridge two lipids if it is hydrogen bonded to both lipids. The figure shows the interlipid bridges are most prominent at $w_0 = 7$, and at $w_0 = 11$ the numbers seem to decline with the bilayer having the lowest number of interlipid bridges. Similarly intralipid bridging increases up until water-to-lipid ratio 7-11 and remains at that level also in the fully hydrated bilayer. The interlipid and intralipid percentages exhibit analogous behaviour. Notably, only ∼1 hydrogen bond per lipid (corresponding to approximately one fifth of the total number of hydrogen bonds) are involved in interlipid bridging in the simulations. The increase of bridging until some intermediate w_0 level followed by decline in interlipid bridges and leveling off of intralipid bridges indicates that there are two effects at play. First, hydrogen bond bridging increases as a function of water-to-lipid ratio due to the increased number of water molecules present at the headgroup region, see Figure 2. Then, at hydrations above $w_0 = 7$, some effect starts to cut down the amount of interlipid bridges even though the degree of hydrogen bonding of the headgroups actually increases.

To better understand this effect we examined the site dependence of hydrogen bond bridging, see Figure 3. In the simulations, a vast majority of interlipid bridges (58-48 %) were formed between phosphate P=O oxygens. For intralipid bridging, P=O and C=O oxygen bridging is favoured (69-62 %). Furthermore, the decrease in interlipid bridging is localised specifically at the P=O oxygens with bridging to other oxygen atoms remaining relatively unaffected. This behaviour leads us to conclude hydrogen bond bridging is closely related to the packing properties of the polar-apolar interface: decrease in the interfacial curvature increases phosphate group distance while build-up of hydration layer increases area per lipid thus hindering the relatively short-ranged bridging effect. Intralipid bridging on the other hand is not affected by the curvature and hence is unaffected by it. Water dynamics may also influence, but because intralipid bridging shows no signs of this we consider this less likely.

To evaluate water dynamics explicitly, we calculated hydrogen bond correlation functions from the simulations. These are presented in Figure 5. In general, slower decay of the correlation functions implies more stable bonding either due to strong interaction between the bonding species or due to molecular isolation. The figure shows a significant slow-down of hydrogen bond dynamics as w_0 is decreased. Furthermore, the decay is non-exponential with a slowly attenuating tail extending to several nanoseconds – particularly at water-to-lipid ratio $w_0 = 5$.

Next, we integrated the correlation functions to obtain the hydrogen bond lifetimes, see Eq. 2. As the decay of the correlation functions in these systems is non-exponential, these do not provide the actual lifetimes but the values tell about the relative stability of the hydrogen bonds. Figure 6 shows that the correlation times of the hydrogen bonds decrease in the order P=O > C=O > P–O > C–O, although the difference between P=O and C=O oxygens is substantial only for $w_0 = 5$. The observed order of correlation times roughly correlates with the strength of the hydrogen bond estimated from the partial charges and the Lennard-Jones parameters for these sites in the simulational model.

Besides the hydrogen bond strength, Figure 6 shows that the lifetime also depends on the location of the acceptor site. For instance, the number of hydrogen bonds formed to P=O and C=O sites differs substantially yet the lifetimes are almost identical at water-to-lipid ratios 7 and 11. Only at the most dehydrated reverse micelle ($w_0 = 5$) a clear difference in the average lifetime emerges. We interpret this effect to be due to

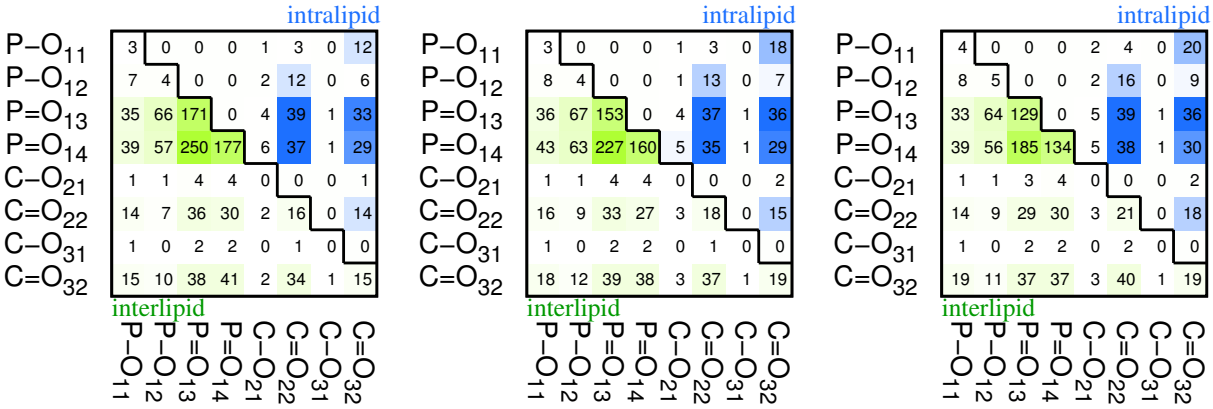

Fig. 4 Average number of interlipid and intralipid bridges per lipid per acceptor site. Interlipid bridges are shown in the lower triangle and along the diagonal in green/white cells and intralipid bridges in the upper triangle as blue/white cells. All numbers are in 1/1000s of the actual number count and a deeper color indicates more bridges. See Fig. 2 for the phosphatidylcholine lipid headgroup and the acceptor oxygen labelling in the graph.

molecular isolation; an increased local hydration, see Fig. 2, results in a more isotropic hydrogen bonding environment and accelerated rotational dynamics, as well as, donor exchange. On the other hand, isolated water molecules have only the lipid acceptor sites to bond with. Indications of similar, local hydration dependence on hydrogen bond stability can be seen to a lesser extent for the C=O oxygens as well as P–O oxygens. For these, the effect is smeared by the fact that correlation times calculated from the smaller reverse micelles RM57 ($w_0 = 7$) and RM97 ($w_0 = 11$) are generally slightly shorter than those calculated from the larger aggregates at the same water-to-lipid ratio. This is likely a result from the greater amount of shape fluctuations the smaller reverse micelles undergo. Deduction concerning the acceptor sites C–O_{21} and C–O_{31} suffers from the low hydration at these sites.

Figure 5 presents also the correlation functions of hydrogen bond bridges. Because a bridge requires two hydrogen bonds, the bridge correlation functions are expected to decay faster than lipid - water correlation functions. Curiously, however, the data shows bridge correlation functions decay only slightly faster, indicating that hydrogen bond bridges are long-lived rather than transient. As the systems contain only $\sim$1 hydrogen bond bridge per lipid, the raw data contains noise which would reflect significantly on integrated bridge lifetimes. Therefore, we have not evaluated the relative stability by integration. However, the correlation functions show two partially overlapping bands of lipid bridges at water-to-lipid ratios $w_0 = 11$ and $w_0 = 28$. This signifies a set of hydrogen bond bridges has significantly longer lifetimes than the bridges corresponding to the faster decaying band. Careful analysis reveals the slower band corresponds to bridges involving the phosphate group. As a consequence, hydrogen bond bridges that have oxygens from phosphate group as one of the binding sites have substantially slower dynamics than bridges between acceptor sites closer to the tails. This indicates that only bridges originating from the phosphate group form persistent hydrogen bond structures. In total, the observed dynamic behaviour of the hydrogen bond bridges indicates that bridging is strongly affected by hydration and increasing it makes the bridges more transient.

4 Discussion

In this work, we applied all-atom molecular dynamics to study the relation between lipid hydration and reverse micelle structure in organogel forming phosphatidylcholine lipid/water/cyclohexane system. We characterised lipid-water hydrogen bonds at three water-to-lipid ratios and assessed the sensitivity to aggregation number. We find the hydrogen bond network, bonding strength, as well as hydrogen bond bridging and bridge stability depend strongly on the specific site and local hydration. Most notably, increased access to water molecules makes the hydrogen bonding more transient, enhances local water dynamics at the reverse micelle cores, and decreases the amount and persistence of water bridges formed between two lipids. These findings allow us to present a microscopic picture of the gelation process, as well as, discuss the implications this has for other lecithin organogels.

To our knowledge hydration of phosphatidylcholines in reverse micellar environment has not been previously studied using molecular dynamics. However, a number of studies detailing the hydrogen bond network in bilayers at a molecular level have been published. According to these simulational studies, water binding is localised to the phosphate groups (specifically to P=O oxygens) while carbonyl groups located deeper into the interface are bonded to a much lesser

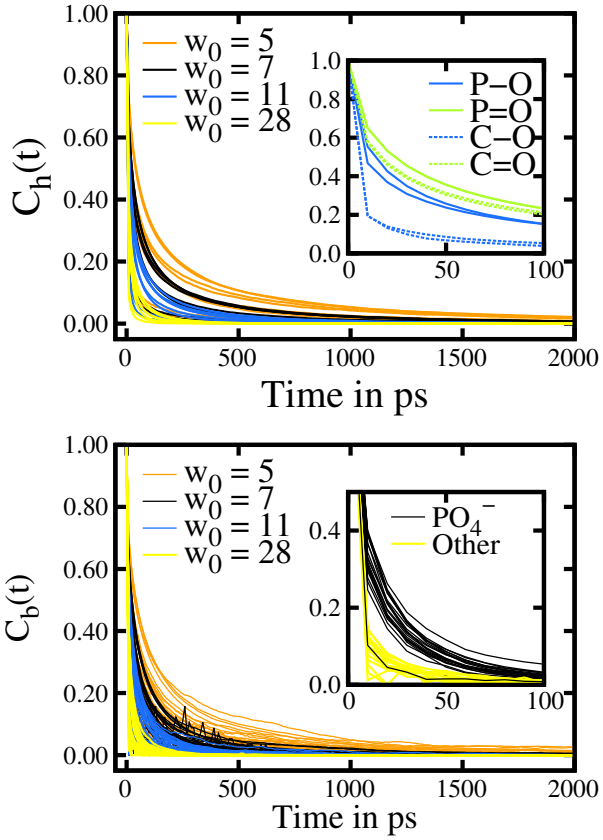

Fig. 5 Hydrogen bond correlation functions (top panel) and hydrogen bond bridge correlation functions (bottom panel). Inserts present a comparison of the hydrogen bond and bridge correlations between phosphate acceptor sites and the other acceptor sites (tail-tail sites) for water-to-lipid ratios $w_0 = 11$ and $w_0 = 28$ in the fast time scale (up to 100 ps time) showing the significant slow-down of hydrogen bond dynamics in reverse micellar cores in comparison to a hydrated bilayers. See Fig. 2 for the phosphatidylcholine lipid head group and the acceptor oxygen labelling in the graph. In the case of bridge correlations black color indicates that the bridge originates from phosphate group PO_4^-.

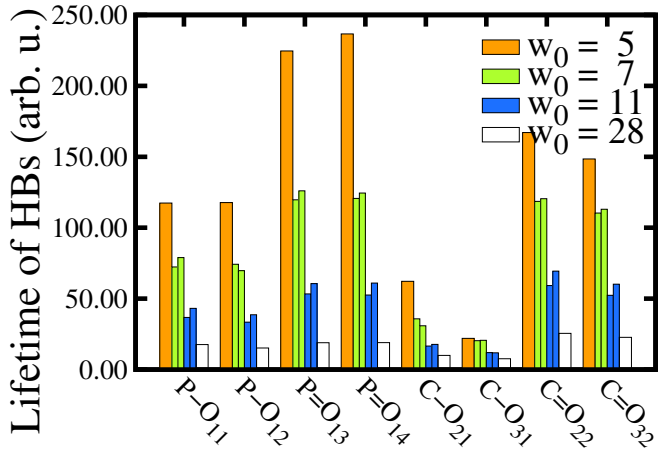

Fig. 6 Integrated lifetimes of hydrogen bonds (HBs) formed to different acceptor oxygens. Lifetimes are expressed in arbitrary units (arb. u.) due to the non-exponential decay of the correlation functions. See Fig. 2 for the phosphatidylcholine lipid head group and the acceptor oxygen labelling in the graph.

degree[42–44]. Water has been reported to form 5.3-7.6 hydrogen bonds with phosphatidylcholines depending on the area per lipid (or temperature and chain unsaturation)[43–47]. This is comparable to the average number of hydrogen bonds $4.8 - 6.1$ calculated from our reverse micelle simulations (7.1 for the bilayer). Therefore, we find the hydration in reverse micelles reported here closely follows the overall phosphatidylcholine hydration behaviour in membranes. Although this close match with bilayer hydration may result from the lipid model being parametrised for bilayers, we find it very reasonable that hydration characteristics of neutral lipids in reverse micelle and bilayer geometries do not deviate significantly at moderate water-to-lipid ratios.

In the simulated reverse micelles, the amount of hydrogen bonding to water follows directly from lipid headgroup hydration. However, the analysis shows also that the lifetime of the hydrogen bonds depend not only on the site but also the local water density at the site; competition between water molecules sped up the dynamics whereas slow-down was observed at sites of low hydration. At low water-to-lipid ratio, the slow-down is even more pronounced. Priorly, Lopez et al.[42] have characterised hydrogen bond dynamics in dimyristoyl phosphatidylcholine bilayer using a simulations method similar to this work. Based on a single simulation they postulated very much in line with our observations that the observed differences in hydrogen bond lifetimes depend not only on the strength of the water-lipid hydrogen bond in question but also on the local water density due to the competition between neighbouring water molecules[42]. For instance, hydrogen bonds to C=O oxygens in their simulations have a longer lifetime than hydrogen bonds to chemically similar P=O oxygens because less water molecules penetrate to the depth of the glycerol moieties and consequently there is less competition between water molecules for the C=O oxygens.

We found lipid bridging by water molecules is present in the reverse micelle system. The simulations showed lipid bridging increases with water-to-lipid ratio at low hydration but increasing the amount of available water molecules quickly saturates the intralipid bridging and turns the amount of interlipid bridging in the system to a decline. Priorly, the presence of hydrogen bond bridging in neutral lipid membranes has been demonstrated both experimentally[48,49] and compu-

tationally[42,43]. In general, computational studies report the number of interlipid bridges in hydrated phosphatidylcholine membranes to be between $0.7-1.7$ bridges per lipid with the exact value depending on the lipid and the simulation conditions, see e.g. Refs.[43,47,50,51]. Comparing these numbers directly to reverse micelles is not reasonable due to the significantly lower hydration in reverse micelle systems. Our bilayer simulation, however, presents noticeably less bridging presumably due to the greater area per lipid of the distearidonoyl phosphatidylcholine (DSPC) in comparison to more saturated lipids.

To our knowledge, bridging in partially hydrated membranes has not been considered computationally. However, Stępniewski et al. compared hydrated gel-phase distearoyl phosphatidylcholine bilayer to liquid crystalline dilinoleyl phosphatidylcholine and found that water molecules in the more contracted distearoyl phosphatidylcholine membrane have a greater tendency towards bridging even though the amount of hydrogen bonds and bridges was actually lower[51]. Additionally, experimental papers discuss bridging in crystalline phosphatidylcholine lipid bilayers. For instance, Volkov et al. confirmed the presence of bridged water molecules in lipid bilayers at low hydration ($w_0 = 0.5-2$) using two-color pump-probe experiments[48] while Pearson and Pascher found using crystallography that in crystalline phosphatidylcholine dihydrate samples phosphate groups and water molecules form infinitely long ribbons along one of the crystal axis[49]. The observed bridging corresponds to one bridge per lecithin molecule[49]. Curiously, our simulations of the reverse micelle system show also approximately one hydrogen bond per lipid.

Lipid hydration has an interesting connection to the gelation transition of phospholipids in oil. Gelation corresponds to the lipids self-assembling (packing) into long, wormlike micelles that entangle in the solution. In general, phospholipids solvated by oil adopt an effectively inverted cone shape which packs as more or less spherical reverse micelles. As the phosphorylcholine group hydration increases, the effective shape of the lipid becomes more cylindrical. This promotes an increase of the aggregation number of the reverse micelle. At first this leads into an elongation of the micelle into a cylinder and at more cylindrical lipid shapes to more lamellar type assembly. On the other hand, an increase in the effective size of the tails typically caused by increasing temperature has an opposite effect. If the cylindrical micelles are long enough to entangle, gelation occurs. Naturally, the precise size distribution of the aggregates in the system is determined by the interplay of the packing considerations and entropy.

Related to this packing consideration, priorly, lipid bridging has been connected with the organogel transition of lecithin reverse micelles in heptane by Shchipunov and Shumilina[13]. Zhao et al.[22] have claimed interlipid bridging plays a role in changing the surfactant packing analogous to lecithin/water/heptane systems also in cyclohexane. The conclusion of Shchipunov and Shumilina in their study of lecithin/heptane organogels was that the formation of hydrogen bond bridges stabilises the cylindrical structure of wormlike reverse micelles (i.e. increases aggregation number and the penalty involved in forming additional end-caps as opposed to elongating the cylindrical miselle.)[13]. This implies the bridging acts dominantly in the cylindrical section. Otherwise, the driving force to elongate the aggregates due to bridging would not exist. Bridging dominantly at the cylindrical section is actually quite plausible to occur in lecithin reverse micelles as the linear strips of bridged lecithin molecules in crystalline lecithin samples are planar[49]. If bridging in lecithin reverse micelles follows same orientation preference, such planar arrangement is feasible axially in the reverse micelle but not at the caps where non-planar bridging is enforced due to geometry.

In experiments, the average length and cross-sectional radius of the reverse micelles, and consequently the aggregation number, increases with increasing water-to-lipid ratio. This implies that the energetic penalty associated with the formation of end-caps, the end-cap energy, also increases relative to the cylindrical section. If hydrogen bond bridges indeed bind neighbouring lecithin molecules together in the cylindrical micelles when gelation occurs, one would expect the amount of hydrogen bond bridges at the very least to remain constant, if not increase, as a function of water-to-lipid ratio. However, our simulations show signs of this kind of behaviour only for $w_0 < 7$ while for water-to-lipid ratios above 7 the bridging decreases noticeably. We remind the reader that in cyclohexane, the reverse micelle organogel maximum viscosity is attained at $w_0 \approx 11$. Hence the experimental viscosity behaviour and amount of bridging in our simulations do not seem to correlate. This signifies that the aggregate elongation in cyclohexane must be influenced if not controlled by some other factor.

Contrary to the amount of bridging, the amount of water-lipid hydrogen bonds seems to correlate with the organogel viscosity behaviour. At these low water-to-lipid ratios, increase in the amount of hydrogen bonds is connected to hydration layer formation. The build-up of a hydration layer, or actually more specifically the space required by the bound water molecules, changes the effective shape of the lipids in cyclohexane toward a more cylindrical effective packing. This contributes to the increase of the aggregation of the reverse micelles, and at suitable lipid effective packing form, to gelation. Hence, instead of bridging, our results suggest that the growth of wormlike reverse micelles in cyclohexane is mainly due to the formation of a hydration layer around lipid headgroups. Nevertheless, bridging is still present, and contributes to the aggregate stability also in cyclohexane – it is merely not the dominant factor at water-to-lipid ratios significantly above

5 where the reverse micelles in cyclohexane gelate. Actually, our results suggest that bridging becomes dominant only when water molecules are effectively isolated from one another, as in the low water-to-lipid ratios where lecithin reverse micelles in heptane gelate. Hence, this picture is consistent with bridging contributing significantly in the heptane/lecithin system and the gelation effect there seeming to be connected to the bridging capability of the gelation agent. Based on our hydrogen bond and bridge dynamics results, we postulate that in the heptane system the bridging dynamics is likely to be significantly slower than in the cyclohexane, thus making the influence of bridging larger.

As for the observed decrease in bridging with increasing water-to-lipid ratio, we suggest two possible explanations. Firstly, the increased amount of water at the headgroup region leads to increased exchange of hydrogen bond donor-acceptor pairs thus disrupting the bridging. Indeed, our results and those of others[42,52] indicate that increase in local water density leads to increased water dynamics at phospholipid interfaces. The other possible explanation is that bridging is feasible only on a relatively narrow range of acceptor-acceptor distances and subtle changes in it due to for example increased hydration can cause bridging to become unfavourable. We cannot say conclusively which of these is the cause. However, the saturation of intralipid bridging indicates that the dynamics may have less influence than the geometric considerations. These factors, as well as, the fact that small changes in solvent nature is enough to hinder or promote aggregate growth indicates that bridging is a relatively weak effect. For comparison, alkaline earth and rare earth cations thought to induce gelation via electrostatics mediated salt bridges are much more insensitive to solvent gelating both cycloalkanes and alkanes at low ion-to-lipid ratio[11,12].

The picture emerging from our simulations that the hydration directly modifies the lipid packing properties without major contribution from bridging is contrary to the deductions of Zhao et al.[22]. They inferred similar bridging structure as in heptane[13] is present also in the cyclohexane system[22]. We believe the reason for this discrepancy is that the IR data of Zhao et al. shows directly that the hydrogen bondedness of the lipid headgroup phosphate group is linked to the shape of the reverse micelle, but does not, as such, indicate the presence or absence of bridging. Hence, the interpretation of the role of interlipid bridging based on these experiments is challenging, and relies partially on the experimental results of Shchipunov and Shumilina on heptane systems[13] where interlipid bridging was deduced by correlating gelation agent chemical structure with their ability to induce gelation. This provides a significantly more direct connection to bridging. As the work of Zhao et al. concentrated on water induced organogel formation with carbon dioxide as control, no similar correlation could be demonstrated. Finally, we point out that our suggested model of the hydration layer formation driving the gelation transition in cyclohexane explains the observations of Zhao et al., as well as, the bridging model at lower hydration (as is in heptane).

5 Conclusions

In summary we have conducted all-atom simulations of phosphatidylcholine reverse micelles in cyclohexane to study the mechanism behind water induced organogel formation. The findings clarify the role of packing constraints (shape of the lipid) and specific interactions (in particular, hydrogen bond bridging) to the formation of lecithin organogels. Namely, we deduced that in cyclohexane/lecithin system hydrogen bond bridging plays a relatively minor role in the formation of the organogel. Instead, the effective shape of the lipid controls the form of the wormlike reverse micelles and the viscosity of the resulting solution. The effective shape of the lipid, in turn, is influenced by the number and location of water-lipid hydrogen bonds. Even if in minor role in gelation, our results do, however, indicate that at low water-to-lipid ratios ($w_0 < 5$) bridging becomes the dominant form of hydrogen bonding.

We also report a significant slow-down of the dynamics of the system in terms of water mobility and hydrogen bond stability at low hydration. The result originates directly from the lack of plasticizing water molecules. All in all, the simulations show that besides the usually considered physical dimensions of the reverse micelles, also the dynamics in the microenvironment provided by the core can be controlled by hydration. This could bear significance in designing, e.g., catalysis platforms, controlling synthesis, or molecular separation and encapsulation.

The study is, to our knowledge, the first computational characterization of the role of hydration in lecithin organosols or gels. The results show molecular simulations are able to provide detailed information on the hydration response of these complicated, dynamic systems and to generate understanding on the nature of the organogel transition at a solvent-specific level.

Acknowledgements

This research was supported by Fortum Foundation, Academy of Finland, and a Marie Curie Career Integration Grant within the 7th European Community Framework Programme (grant agreement 293861). Computational resources by CSC IT Centre for Science, Finland, are gratefully acknowledged.

References

1 S. Xu, H. Zhou, J. Xu and Y. Li, *Langmuir*, 2002, **18**, 10503–10504.

2 L. Qi, J. Ma, H. Cheng and Z. Zhao, *The Journal of Physical Chemistry B*, 1997, **101**, 3460–3463.
3 H. Shi, L. Qi, J. Ma and H. Cheng, *Chem. Commun.*, 2002, 1704–1705.
4 Q. Peng and P. L. Luisi, *European Journal of Biochemistry*, 1990, **188**, 471–480.
5 R. Scartazzini and P. L. Luisi, *The Journal of Physical Chemistry*, 1988, **92**, 829–833.
6 P. Schurtenberger, R. Scartazzini, L. J. Magid, M. E. Leser and P. L. Luisi, *The Journal of Physical Chemistry*, 1990, **94**, 3695–3701.
7 P. Schurtenberger, L. J. Magid, S. M. King and P. Lindner, *The Journal of Physical Chemistry*, 1991, **95**, 4173–4176.
8 P. Schurtenberger and C. Cavaco, *Langmuir*, 1994, **10**, 100–108.
9 S.-H. Tung, Y.-E. Huang and S. R. Raghavan, *Journal of the American Chemical Society*, 2006, **128**, 5751–5756.
10 C.-W. Njauw, C.-Y. Cheng, V. A. Ivanov, A. R. Khokhlov and S.-H. Tung, *Langmuir*, 2013, **29**, 3879–3888.
11 H.-Y. Lee, K. K. Diehn, S. W. Ko, S.-H. Tung and S. R. Raghavan, *Langmuir*, 2010, **26**, 13831–13838.
12 H.-Y. Lee, K. Hashizaki, K. Diehn and S. R. Raghavan, *Soft Matter*, 2013, **9**, 200–207.
13 Y. A. Shchipunov and E. V. Shumilina, *Materials Science and Engineering: C*, 1995, **3**, 43–50.
14 G. Palazzo, *Soft Matter*, 2013, **9**, 10668–10677.
15 D. Capitani, A. L. Segre, F. Dreher, P. Walde and P. L. Luisi, *The Journal of Physical Chemistry*, 1996, **100**, 15211–15217.
16 R. Angelico, A. Ceglie, U. Olsson and G. Palazzo, *Langmuir*, 2000, **16**, 2124–2132.
17 P. Schurtenberger, G. Jerke, C. Cavaco and J. S. Pedersen, *Langmuir*, 1996, **12**, 2433–2440.
18 D. Capitani, E. Rossi, A. L. Segre, M. Giustini and P. L. Luisi, *Langmuir*, 1993, **9**, 685–689.
19 R. Angelico, G. Palazzo, G. Colafemmina, P. A. Cirkel, M. Giustini and A. Ceglie, *The Journal of Physical Chemistry B*, 1998, **102**, 2883–2889.
20 R. Angelico, S. Amin, M. Monduzzi, S. Murgia, U. Olsson and G. Palazzo, *Soft Matter*, 2012, **8**, 10941–10949.
21 R. Angelico, A. Ceglie, G. Colafemmina, F. Delfine, U. Olsson and G. Palazzo, *Langmuir*, 2004, **20**, 619–631.
22 Y. Zhao, J. Zhang, Q. Wang, W. Li, J. Li, B. Han, Z. Wu, K. Zhang and Z. Li, *Langmuir*, 2010, **26**, 4581–4585.
23 E. Shumilina, Y. Khromova and Y. Shchipunov, *Russian Journal of Physical Chemistry*, 2000, **74**, 1083–1092.
24 G. Cavallaro, G. L. Manna, V. Liveri, F. Aliotta and M. Fontanella, *Journal of Colloid and Interface Science*, 1995, **176**, 281 – 285.
25 A. V. Martinez, L. Dominguez, E. Małolepsza, A. Moser, Z. Ziegler and J. E. Straub, *The Journal of Physical Chemistry B*, 2013, **117**, 7345–7351.
26 S. Abel, F. Sterpone, S. Bandyopadhyay and M. Marchi, *The Journal of Physical Chemistry B*, 2004, **108**, 19458–19466.
27 S. Abel, M. Waks, M. Marchi and W. Urbach, *Langmuir*, 2006, **22**, 9112–9120.
28 S. Vierros and M. Sammalkorpi, *The Journal of Chemical Physics*, 2015, **142**, 094902.
29 B. Hess, C. Kutzner, D. van der Spoel and E. Lindahl, *Journal of Chemical Theory and Computation*, 2008, **4**, 435–447.
30 S. Pronk, S. Pall, R. Schulz, P. Larsson, P. Bjelkmar, R. Apostolov, M. R. Shirts, J. C. Smith, P. M. Kasson, D. van der Spoel, B. Hess and E. Lindahl, *Bioinformatics*, 2013, **29**, 845–854.
31 A. D. MacKerell, D. Bashford, Bellott, R. L. Dunbrack, J. D. Evanseck, M. J. Field, S. Fischer, J. Gao, H. Guo, S. Ha, D. Joseph-McCarthy, L. Kuchnir, K. Kuczera, F. T. K. Lau, C. Mattos, S. Michnick, T. Ngo, D. T. Nguyen, B. Prodhom, W. E. Reiher, B. Roux, M. Schlenkrich, J. C. Smith, R. Stote, J. Straub, M. Watanabe, J. Wiórkiewicz-Kuczera, D. Yin and M. Karplus, *The Journal of Physical Chemistry B*, 1998, **102**, 3586–3616.
32 J. B. Klauda, R. M. Venable, J. A. Freites, J. W. O'Connor, D. J. Tobias, C. Mondragon-Ramirez, I. Vorobyov, A. D. MacKerell and R. W. Pastor, *The Journal of Physical Chemistry B*, 2010, **114**, 7830–7843.
33 O. Guvench, S. N. Greene, G. Kamath, J. W. Brady, R. M. Venable, R. W. Pastor and A. D. Mackerell, *Journal of Computational Chemistry*, 2008, **29**, 2543–2564.
34 I. Vorobyov, V. M. Anisimov, S. Greene, R. M. Venable, A. Moser, R. W. Pastor and A. D. MacKerell, *Journal of Chemical Theory and Computation*, 2007, **3**, 1120–1133.
35 U. Essmann, L. Perera, M. L. Berkowitz, T. Darden, H. Lee and L. G. Pedersen, *The Journal of Chemical Physics*, 1995, **103**, 8577–8593.
36 B. Hess, H. Bekker, H. J. C. Berendsen and J. G. E. M. Fraaije, *Journal of Computational Chemistry*, 1997, **18**, 1463–1472.
37 S. Miyamoto and P. A. Kollman, *Journal of Computational Chemistry*, 1992, **13**, 952–962.
38 G. Bussi, D. Donadio and M. Parrinello, *The Journal of Chemical Physics*, 2007, **126**, 014101.
39 M. Parrinello and A. Rahman, *Journal of Applied Physics*, 1981, **52**, 7182–7190.
40 W. Humphrey, A. Dalke and K. Schulten, *Journal of Molecular Graphics*, 1996, **14**, 33–38.
41 D. Rapaport, *Molecular Physics*, 1983, **50**, 1151–1162.
42 C. F. Lopez, S. O. Nielsen, M. L. Klein and P. B. Moore, *The Journal of Physical Chemistry B*, 2004, **108**, 6603–6610.
43 M. Pasenkiewicz-Gierula, Y. Takaoka, H. Miyagawa, K. Kitamura and A. Kusumi, *The Journal of Physical Chemistry A*, 1997, **101**, 3677–3691.
44 S. Leekumjorn and A. K. Sum, *Biophysical Journal*, 2006, **90**, 3951 – 3965.
45 A. H. de Vries, A. E. Mark and S. J. Marrink, *The Journal of Physical Chemistry B*, 2004, **108**, 2454–2463.
46 P. Niemelä, M. T. Hyvönen and I. Vattulainen, *Biophysical Journal*, 2004, **87**, 2976 – 2989.
47 T. Rog, K. Murzyn, J. Milhaud, M. Karttunen and M. Pasenkiewicz-Gierula, *The Journal of Physical Chemistry B*, 2009, **113**, 2378–2387.
48 V. V. Volkov, D. J. Palmer and R. Righini, *The Journal of Physical Chemistry B*, 2007, **111**, 1377–1383.
49 R. H. Pearson and I. Pascher, *Nature*, 1979, **281**, 499 – 501.
50 K. Murzyn, T. Róg, G. Jezierski, Y. Takaoka and M. Pasenkiewicz-Gierula, *Biophysical Journal*, 2001, **81**, 170 – 183.
51 M. Stępniewski, A. Bunker, M. Pasenkiewicz-Gierula, M. Karttunen and T. Róg, *The Journal of Physical Chemistry B*, 2010, **114**, 11784–11792.
52 T. Róg, K. Murzyn and M. Pasenkiewicz-Gierula, *Chemical Physics Letters*, 2002, **352**, 323 – 327.